Novel Encapsulation of Cadmium Orthostannate Nanoparticles with 3-(mercaptopropyl)trimethoxysilane : Synthesis, Characterisation, and Application

Dr Lu Yong[1], Mr Zheng Long[2], Yu Youjing, Wang Ziying, Zhou Ya Nan[3i], Dr Shah Kwok Wei[4]

1. Background and Purpose of the Research

Metal nanoparticles (MNPs) and nano-sized metal oxides (NMOs) have drawn worldwide attention in recent years because of their high potential in environmental science [1] - in particular, their applications in building construction for thermal insulation [2] due to their infrared radiation (IR) reflecting and absorbing ability [3-5]. Such nanoparticles (NPs) can be employed in construction materials to reduce energy use for indoor passive cooling [6-7]. Amongst these NPs, Cadmium Orthostannate (Cd_2SnO_4) NPs are known for their promising IR reflecting and absorbing ability [8-10], low cost in production [11] and chemical stability [12]. Therefore, novel materials based on Cd_2SnO_4 NPs would be promising for building applications.

However, as bare NPs exhibit poor dispersion in water as a result of easy aggregation, the applications of bare NPs are thus limited. One favorable approach to overcome this drawback is by employing the 'core-shell' structure. Consequently, NPs with silica coating have been widely explored with the aim to enhance their dispersion. Moreover, numerous results have shown that after altering their surface chemistry through coating [13], NPs' resistance to oxidation is reinforced [14], while the risks of inhalation and toxicity are considerably reduced [15]. As a result, the successfully prepared silica-coated NPs have been widely investigated in surface-enhanced Raman scattering (SERS), catalytic, colorimetric, and optical applications [16].

There are several synthetic methods of silica coating and various silane precursors such as tetramethyl orthosilicate (TMOS) and Tetraethyl orthosilicate (TEOS). However, these silanes are usually insoluble in water [17-18], resulting in difficulty for hydrolysis and thus a necessity to use alcohol as the co-solvent. It is known that if a methoxyl group in TMOS is replaced by a mercaptopropyl group, the resulting molecule, 3-(mercaptopropyl)trimethoxysilane (MPTMS, $HS(CH_2)_3–Si–(OCH_3)_3$), will have certain solubility in water, facilitating the hydrolysis process prior to condensation [19-21]. Therefore, compared to TMOS and TEOS, MPTMS is a more environmentally-friendly material because silica coating can easily take place in aqueous solution. In addition, it is also desirable that the thiol group (–SH) in such precursor can directly bind onto the surface of NPs via the strong metal-thiol interaction [22], allowing effective silica coating on NPs to be facilely achieved at room temperature.

Intensive researches have been done on synthesizing silica-coated MNPs using MPTMS for biological and magnetic applications [23-25]. However, silica coating using MPTMS has been insufficiently tested on Cd_2SnO_4. Herein, this project focuses on the preparation of silica-coated Cd_2SnO_4 @SiO_2 NPs, using MPTMS as a precursor, as well as their characterization for possible thermal applications. Additionally, a number of various MNPs and NMOs have also been tested for silica coating via the same method (**Appendix b&c**).

[1] Research Assistant, Department of Building, National University of Singapore
[2] PhD student, Department of Building, National University of Singapore
[3] Student, Hwa Chong Institution (Junior College Section)
[4] Associate Professor, Department of Building, National University of Singapore

2. Hypotheses

Cd_2SnO_4 NPs can be successfully coated with MPTMS to form core-shell structure at optimal NP to MPTMS ratio. Successfully coated Cd_2SnO_4@SiO_2 NPs exhibit better dispersion than bare NPs. Cd_2SnO_4@SiO_2 NPs also exhibit novel thermal shielding ability when being applied onto building materials.

3. Methods and Materials

3.1 Materials

3-(mercaptopropyl)trimethoxysilane (MPTMS, 95%) and Cd_2SnO_4 NPs were used as received from Sigma-Aldrich and EasChem respectively. Ammonia solution (25 wt%; EMSURE) and acetone (99%; APC) were also used as received. Water-based Polyurethane (WPU; Trasco Coating) was used when applying NPs onto glass slides. Deionised (DI) water was used throughout all experiments (**Appendix a**).

3.2 Synthesis of Cd_2SnO_4@SiO_2 NPs

10 µl/mL MPTMS stock solution was prepared by hydrolysing 250 µL of MPTMS in 25 mL of deionised (DI) water overnight using a magnetic stirrer (**Fig. 1a**)(**Appendix d**). 1 mL of the stock solution was then mixed with 5 mg of Cd_2SnO_4 NPs in a glass vial. Another 2 mL of DI water was added to modify the ratio of Cd_2SnO_4 to MPTMS to 1 mg to 2 µL (**Fig. 1b**). The mixture was continuously shaken in ultrasonic bath for 15 minutes (**Fig. 1c**). Subsequently, 30 µL of ammonia was added into each glass vial (**Fig. 1d**), followed by dispersion using ultrasonic bath for 60 minutes for the reaction to proceed until a well-dispersed suspension was obtained (pH~10) (**Fig. 1e**)(**Appendix e**). The collected Cd_2SnO_4@SiO_2 NPs were purified by washing with acetone via redispersion-centrifugation at 5000 rpm for 5 minutes for 3 rounds. The obtained Cd_2SnO_4@SiO_2 NPs were redispersed in 3 mL of DI water for further use (**Fig.1f**).

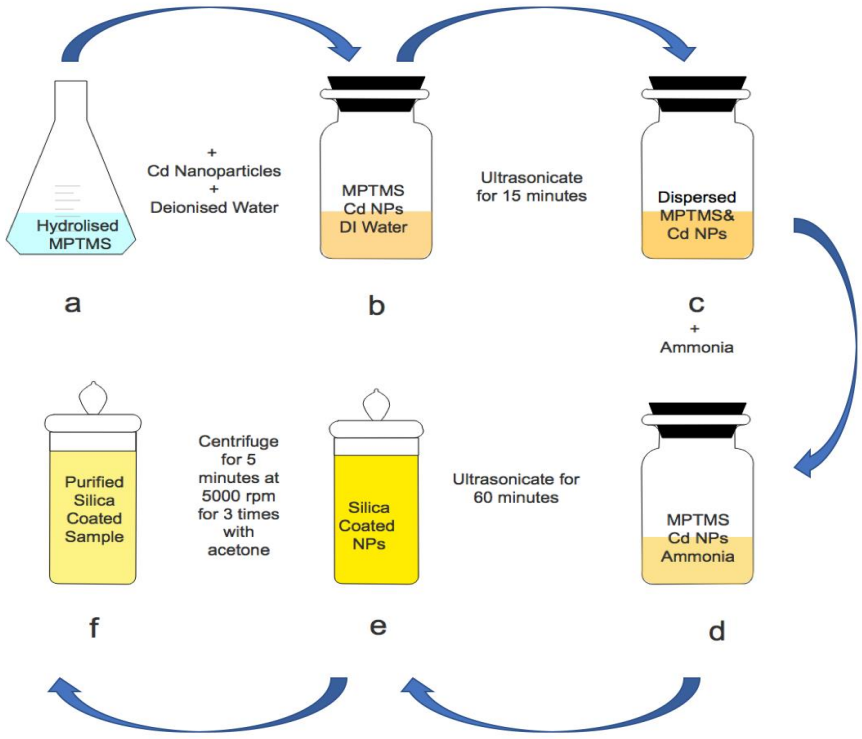

Fig. 1 Schematic procedure for silica coating of Cd_2SnO_4 NPs

3.3 Characterization

3.3.1 Transmission electron microscopy (TEM)

Bright-field transmission electron microscopy (TEM) images of the bare Cd_2SnO_4 NPs and prepared $Cd_2SnO_4@SiO_2$ NPs were taken using a TEM (JEOL, JEM 2010F) machine operated at an accelerating voltage of 300 kV. In preparing the samples, a drop of aqueous solution containing the bare or coated Cd_2SnO_4 NPs was placed onto the surface of a lacey formvar/carbon 300-mesh copper grid (Tian LD, T10023) , and the grid was allowed to dry in air.

3.3.2 Dispersion Test

The dispersions of bare and coated Cd_2SnO_4 NPs in DI water were compared in both two-dimensional (2D) form (glass slides; Menzel-Glaser; 22x22 mm) and three-dimensional (3D) form (glass vials; 2 mL) for a duration of 1 hour. 5 mg of $Cd_2SnO_4@SiO_2$-SH NPs and bare Cd_2SnO_4 NPs were uniformly dispersed in water using ultrasonic bath before applied to glasswares. Equal volume of both suspensions were placed into glass vials and onto glass slides respectively. Both vials and slides were placed against a sheet of white A4 paper and observed for their dispersion in water separately after 1 hour. Photos (using Oppo R9s camera) were taken at the start and after 1 hour respectively to compare their dispersion ability.

3.3.3 UV-vis Absorption

The IR shielding property of $Cd_2SnO_4@SiO_2$ NPs was studied by measuring transmittance of light through the glass slides using a UV-vis-NIR spectrophotometer (Shimadzu UV-3150) in the wavelength range of 200 nm to 3200 nm. The sample was prepared by mixing 5 mg of obtained $Cd_2SnO_4@SiO_2$NPs with 1 mL WPU (250 μL/mL). The mixture was uniformly painted onto a transparent glass slide and let dry in air for 24 hours. A control sample was prepared by uniformly coating 1 mL of 250 μL/mL WPU aqueous solution onto a transparent glass slide.

3.3.4 Temperature Change Test

A temperature change test was subsequently conducted by heating the two sample glass slides with near infrared bulb (RubyLux, NIR-A). The temperature of the glass slides and of the surrounding air directly below the slides were measured and recorded using a thermocouple thermometer (Type J ET-959). An thermal imaging camera (Flir One) was used to illustrate the temperature variation of the surrounding of the setup via infrared images.

4. Results and Discussion

4.1 Synthesis of $Cd_2SnO_4@SiO_2$ NPs

$Cd_2SnO_4@SiO_2$ core–shell structured NPs were prepared by a facile, efficient and economic coating process in alcohol-free aqueous solution at room temperature. Pre-hydrolyzed MPTMS and ammonia were used as a precursor and a cross-linking catalyst respectively. The sufficiently polar mercaptopropyl group in MPTMS facilitated its hydrolysis in water (**Fig. 2a**), followed by the direct surface binding of MPTMS molecules onto Cd_2SnO_4 NPs through strong metal-thiol (M–S) bonds. The addition of ammonia created a desirable alkaline environment (pH~10) for the subsequent condensation of MPTMS to form a network of -O-Si-O- bonds, resulting in the formation of a core-shell structure (**Fig. 2b**). Such a process avoided the usage of alcohol or other organic solvents in the reaction, making aqueous solution an ideal medium for the silica coating. However, an overnight stirring was necessary for the complete hydrolysis of MPTMS in water. Moreover, both the hydrolysis and condensation of MPTMS were carried out under room temperature in the absence of external heat, rendering the entire reaction energy-efficient.

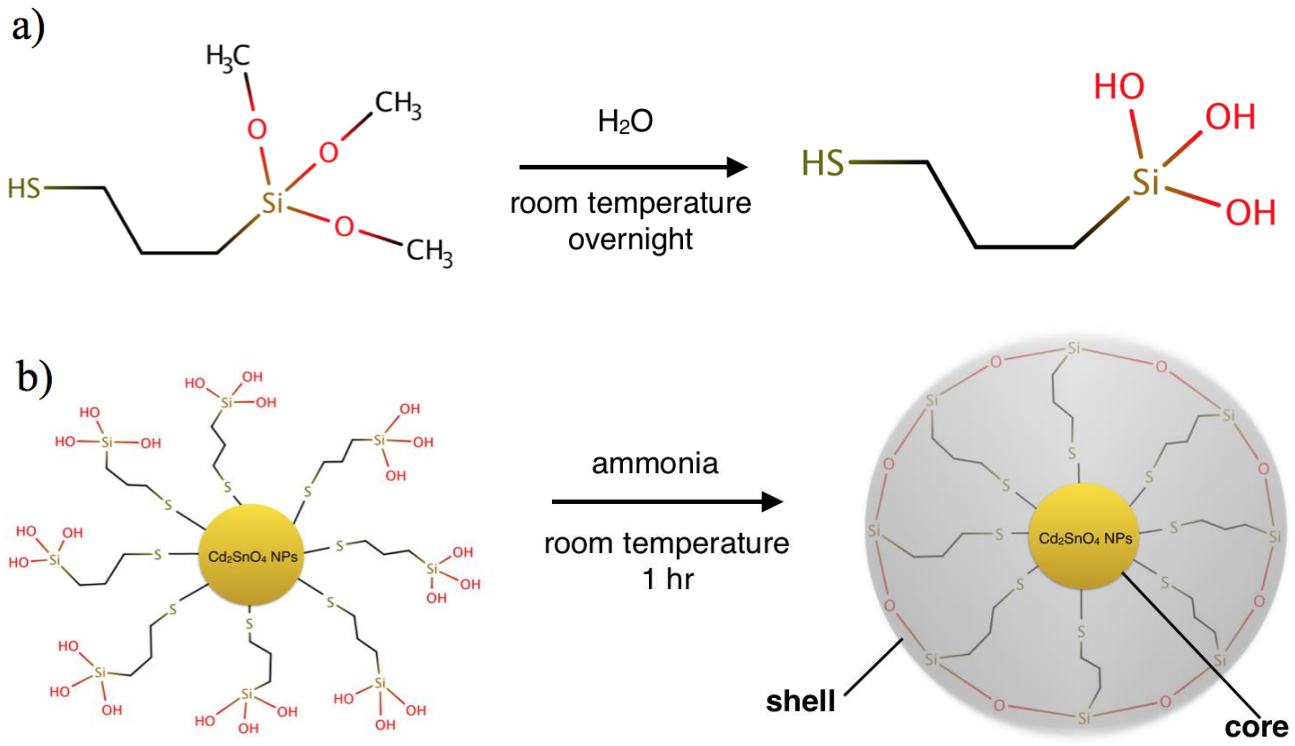

Fig. 2 Schematic illustration of the coating process. a) Hydrolysis of MPTMS. b) Condensation of MPTMS on the surface of Cd_2SnO_4 NPs to form core-shell structure.

4.2 Morphology of Cd_2SnO_4@SiO_2 NPs

As shown in the TEM images (**Fig. 3a-d**), bare Cd_2SnO_4 NPs (~360 nm) were uniformly coated with a silica shell with an average thickness of 40 nm. The shell covered the Cd_2SnO_4 particles thoroughly with a consistent thickness, indicating the successful silica coating by using MPTMS. The TEM measurements herein strongly support the formation of the core-shell structure of Cd_2SnO_4@SiO_2 NPs.

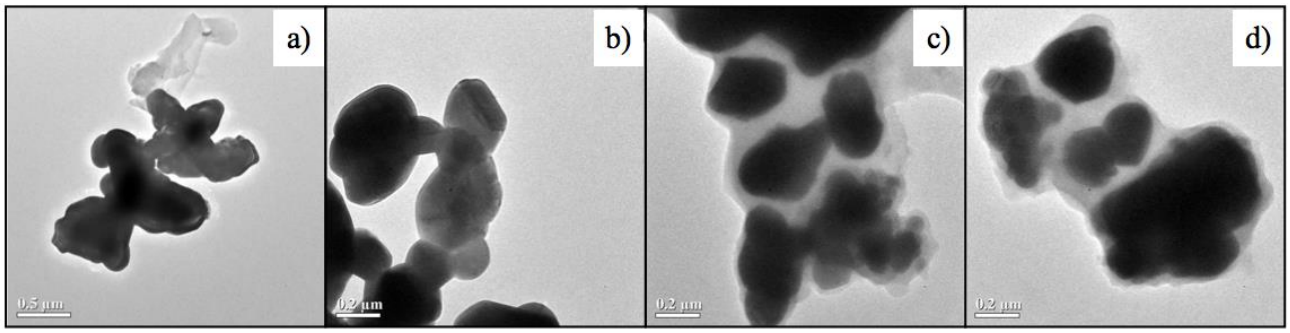

Fig. 3 TEM image of Cd_2SnO_4 NPs before coating (a) & (b) and after silica coating (c) & (d)

4.3 Dispersion of Cd_2SnO_4@SiO_2 NPs

As shown in **Fig. 4-7**, Cd_2SnO_4@SiO_2 NPs have significantly better dispersion property compared to bare Cd_2SnO_4 NPs. After 1 hour of standing, an obvious difference was observed between suspensions of bare Cd_2SnO_4 NPs and Cd_2SnO_4@SiO_2 NPs. It could be seen that most of the uncoated Cd_2SnO_4 NPs settled at the bottom of the glass slide and vial and the solution was transparent (**Fig.5a,7a**), while most of the Cd_2SnO_4@SiO_2 NPs remained dispersed in water **(Fig.5b,7b).** This justified that silica coating tremendously improved the dispersion of Cd_2SnO_4 NPs in water. This

leads to the nobel thermal absorbing and reflecting ability of Cd_2SnO_4@SiO_2 NPs when applied to building materials, as NMOs are now more well dispersed in a given solution.

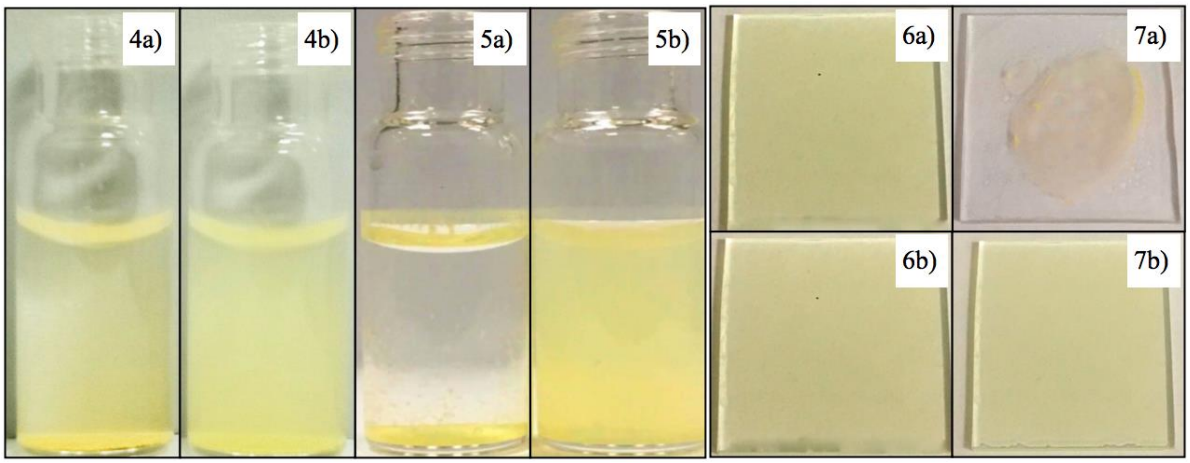

Fig. 4&5a) Cd_2SnO_4 NPs water suspension in glass vial at t=0, 60 min; 5&6b) Cd_2SnO_4@SiO_2 NPs water suspension in glass vial at t=0, 60min. Fig.6&7a) Cd_2SnO_4 NPs water suspension on glass slide at t=0, 60min; 7&8b) Cd_2SnO_4@SiO_2 NPs water suspension on glass slide at t=0, 60min.

4.4 IR transmittance of glass slide coated with Cd_2SnO_4@SiO_2 NPs

A maximum of ~20% decrease (**Fig. 8**, wavelength 700-800 nm; Table 1) and a consistent ~10% decrease (**Fig. 8**, wavelength 1000-1700 nm; Table 1) in transmittance of NIR range is observed of glass slide painted with Cd_2SnO_4@SiO_2 NPs in WPU (test) compared to glass slide painted with bare WPU (control), indicating Cd_2SnO_4@SiO_2 NPs' capability to enhance the heat shielding effect of building materials.

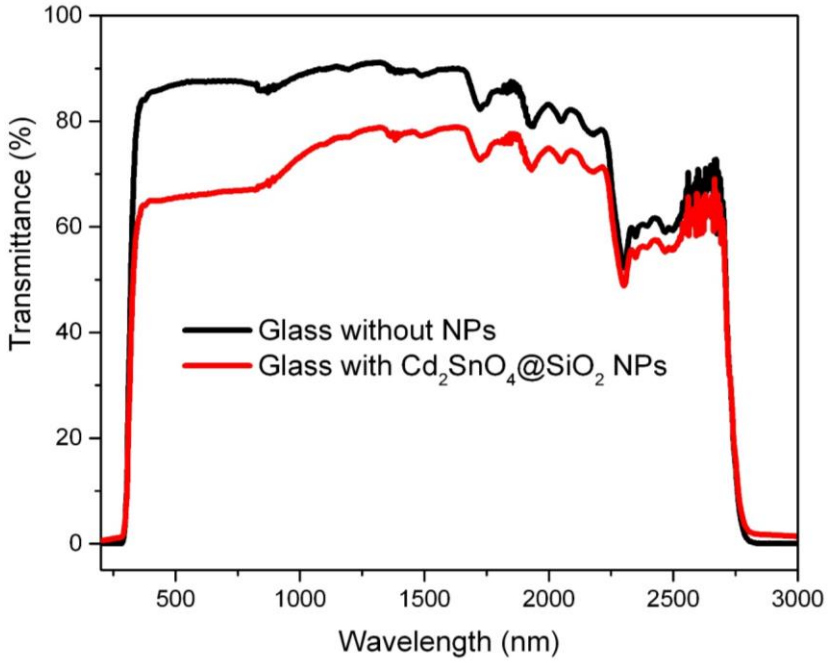

Fig. 8 UV-visible-NIR transmittance spectra of glass slides coated with Cd_2SnO_4@SiO_2 NPs and with bare WPU

Table 1. UV-visible-NIR Transmittance Difference Between Test and Control Samples

Wavelength/nm	Transmittance of Glass without NPs/%	Transmittance of Glass with Coated NPs/%	Transmittance Difference/%
600	87.538	66.077	21.461
800	87.144	67.03	20.114
1000	88.728	73.289	15.439
1200	89.917	77.02	12.897
1400	89.291	77.625	11.666
1600	89.926	78.741	11.185
1800	85.762	76.088	9.674
2000	83.177	74.918	8.259
2200	78.049	70.955	7.094

4.5 Temperature test of glass slide coated with Cd_2SnO_4@SiO_2 NPs

It is further confirmed that building materials painted with Cd_2SnO_4@SiO_2 NPs on the exterior side have enhanced heat shielding ability. After 150 and 210 seconds of heating, the glass slide painted with bare WPU showed a less intense color that represents a lower temperature of 61.0 and 66.4 ℃ respectively under infrared imaging (**Fig.9**) (**Appendix f**), compared to the glass slide painted with Cd_2SnO_4@SiO_2 NPs, which showed a more intense color that represents a higher temperature of 64.5 and 69.2 ℃ respectively. This indicates that Cd_2SnO_4@SiO_2 NPs have novel ability to absorb IR from the heat source, thus preventing drastic temperature rise of building materials they are painted onto.

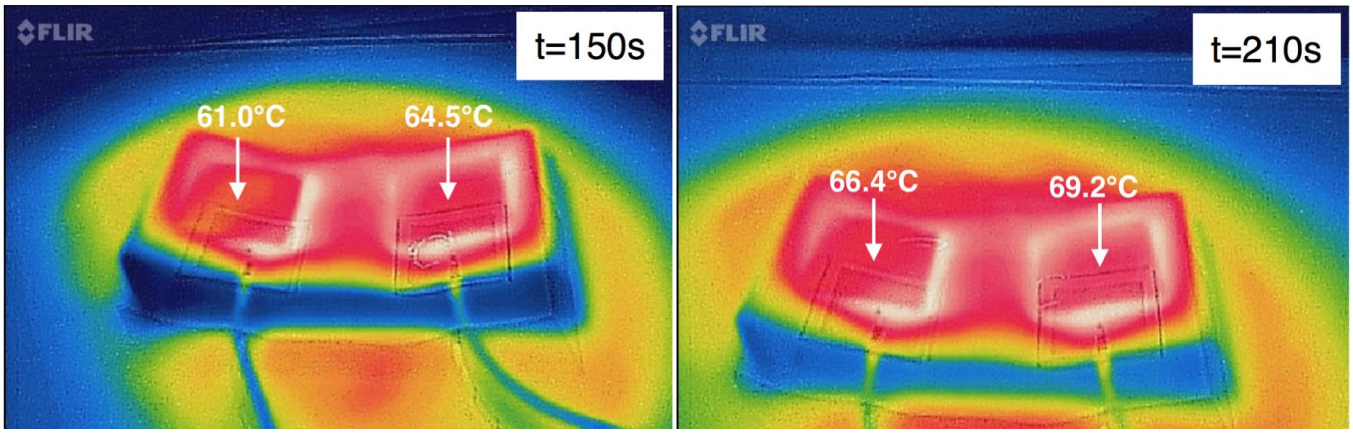

Fig. 9 a&b Infrared images of the surrounding of the glass slides pasted with WPU (a&b left) and WPU+Cd_2SnO_4@SiO_2 NPs (a&b right)

4.6 Temperature rise test of glass slide coated with Cd_2SnO_4@SiO_2 NPs

In order to evaluate the heat absorption and heat transmission of the prepared Cd_2SnO4@SiO_2 NPs, glass slides coated with WPU (sample A), WPU + Cd_2SnO_4 NPs (sample B), WPU + Cd_2SnO_4@SiO_2 (sample C) were prepared. The temperature changes of these glass slides and of the air below glass sides were recorded under irradiation (Table 2 and

Fig. 10 a-d). As it can be seen from Fig 10a & b, glass slides with Cd_2SnO_4@SiO_2 NPs could absorb more heat than the slides without NPs during same period and a maximum temperature difference of 2.7 ℃ could be observed. Similarly, same results were also obtained between the glass slides with Cd_2SnO_4 NPs and with Cd_2SnO_4@SiO_2 NPs and a maximum temperature difference of 7.7 ℃ was demonstrated (Fig. 10 c & d). Herein, it could be concluded that the silica coated Cd_2SnO_4 NPs were more efficient on heat absorption and would be a potential nanofiller in building materials. Energy saving could be expected by using the modified NPs as indoor coating additives. This is in agreement with the dispersion test conducted previously. Sample C exhibited better IR absorbing and reflecting abilities than Sample B because Cd_2SnO_4@SiO_2 NPs are more evenly distributed in WPU solution than bare Cd_2SnO_4 NPs. Another underlying factor could be the dual effect of both the NP core and the silica shell, which reinforce each other in the enhancement of ideal thermal properties.

Table 2. The Heat Absorption and Transmission of Glass Slides Coated with WPU, WPU+ Cd_2SnO_4 NPs and WPU+Cd_2SnO_4@SiO_2 NPs.

	Heat Absorbance		Heat Transmittance	
	General Trend	Max Temperature Difference between samples/°C	General Trend	Max Temperature Difference between samples/°C
Samples A and C	Temperature of C increased at a consistently faster rate	2.7	Temperature of air directly below C increased at a slower rate	4.8
Samples B and C	Temperature of C increased at a consistently faster rate	7.7	Temperature of air directly below C increased at a slower rate	2.3

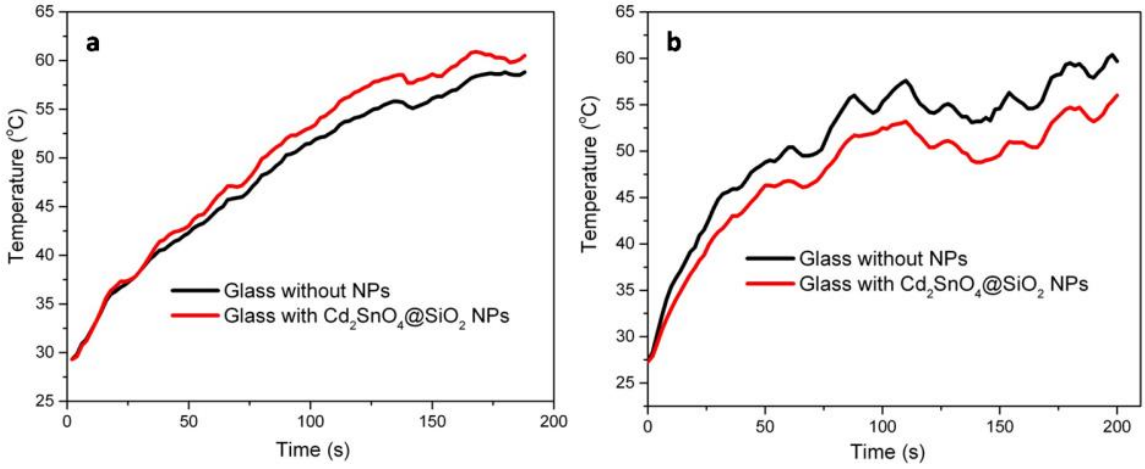

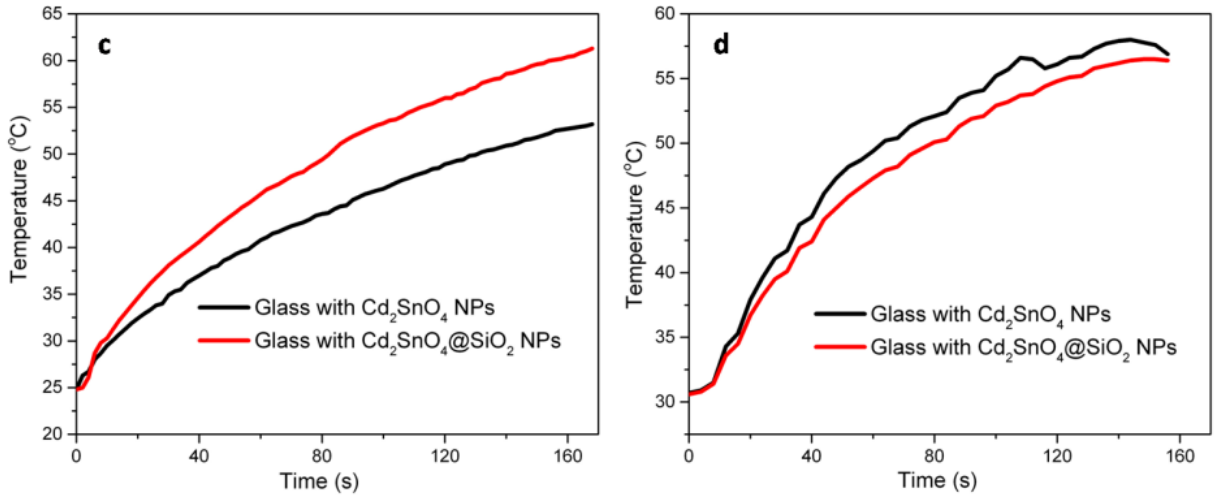

Fig. 10 Heat absorption and heat transmission of coated glass sides. (a) & (c) Temperature changes of coated glass slides. (b) & (d) Temperature changes of the air below glass slides.

5. Conclusion and Recommendations for Future Work

Silica coated Cd_2SnO_4 NPs have been successfully prepared by a feasible and functional process at room temperature in alcohol-free aqueous solution, using MPTMS. Due to the simplicity and efficiency of the silica coating process, Cd_2SnO_4 NPs can be encapsulated in an energy-efficient and environmentally-friendly manner. Further characterisation and investigation of the prepared $Cd_2SnO_4@SiO_2$ NPs in dispersion test, UV-vis-NIR transmittance and temperature change test have confirmed our hypotheses that surface modification of Cd_2SnO_4 NPs could enhance their dispersion and thermal property. A maximum of 20% decrease in NIR transmittance was obtained through the glass slides coated with $Cd_2SnO_4@SiO_2$ NPs, indicating that our prepared material possesses a potential to reduce interior energy use for indoor cooling.

On the other hand, our research work has mainly focused on the thermal property of $Cd_2SnO_4@SiO_2$ NPs. Other desirable traits such as endurance, strength or self-cleaning abilities will also be interesting aspects for exploration because they are potentially useful for building applications as well. Investigation of the coated NPs on different substrate (e.g. plastic, concrete, ceramic) should be carried out and examined in the future, thus expanding the potential of silica coated materials in environmental technology.

6. References

[1] Ngomsik, A.-F., Bee, A., Draye, M., Cote, G. & Cabuil, V. Magnetic nano- and microparticles for metal removal and environmental applications: a review. *Comptes Rendus Chimie* **8,** 963–970 (2005).

[2] Bozsaky, D. Application of Nanotechnology-Based Thermal Insulation Materials in Building Construction. *Slovak Journal of Civil Engineering* **24,** (2016).

[3] Coser, E., Moritz, V. F., Krenzinger, A. & Ferreira, C. A. Development of paints with infrared radiation reflective properties. *Polímeros* **25,** 305–310 (2015).

[4] Jeevanandam, P. *et al.* Near Infrared Reflectance Properties of Metal Oxide Nanoparticles. *The Journal of Physical Chemistry C* **111,** 1912–1918 (2007).

[5] Hildrum, K. *et al.* Near infrared reflectance spectroscopy in the prediction of sensory properties of beef. *Journal of Near Infrared Spectroscopy* **3,** 81 (1995).

[6] Al-Obaidi, K. M., Ismail, M. & Rahman, A. M. A. Passive cooling techniques through reflective and radiative roofs in tropical houses in Southeast Asia: A literature review. *Frontiers of Architectural Research* **3,** 283–297 (2014).

[7] Juvé, V. *et al.* Cooling dynamics and thermal interface resistance of glass-embedded metal nanoparticles. *Physical Review B* **80,** (2009).

[8] Coating technique for reducing surface glare. *Applied Ergonomics* **9,** 252 (1978).

[9] Wolfenden, A. & Donaldson, B. Concise Encyclopedia of Building and Construction Materials. *Journal of Testing and Evaluation* **19,** 178 (1991).

[10] Agnihotri, O. & Raturi, A. Structural electrical and optical properties of CdSxSe1 − x films. *Thin Solid Films* **108,** 313–317 (1983).

[11] Practical Handbook of Photovoltaics. (2012). doi:10.1016/c2011-0-05723-x

[12] http://ljournal.ru/wp-content/uploads/2017/03/a-2017-023.pdf. (2017). doi:10.18411/a-2017-023

[13] Lewis, D. J. & Pikramenou, Z. Lanthanide-coated gold nanoparticles for biomedical applications. *Coordination Chemistry Reviews* **273-274,** 213–225 (2014).

[14] Hu, P., Morabito, J. V. & Tsung, C.-K. ChemInform Abstract: Core-Shell Catalysts of Metal Nanoparticle Core and Metal-Organic Framework Shell. *ChemInform* **46,** (2015).

[15] Chia, S. L. & Leong, D. T. Reducing ZnO nanoparticles toxicity through silica coating. *Heliyon* **2,** (2016).

[16] Shah, K. W. *et al.* Aqueous route to facile, efficient and functional silica coating of metal nanoparticles at room temperature. *Nanoscale* **6,** 11273–11281 (2014).

[17] Siouffi, A.-M. Silica gel-based monoliths prepared by the sol–gel method: facts and figures. *Journal of Chromatography A* **1000,** 801–818 (2003).

[18] Brook, M. A., Chen, Y., Guo, K., Zhang, Z. & Brennan, J. D. Sugar-modified silanes: precursors for silica monoliths. *J. Mater. Chem.* **14,** 1469–1479 (2004).

[19] Engelhardt, H. & Orth, P. Alkoxy Silanes for the Preparation of Silica Based Stationary Phases with Bonded Polar Functional Groups. *Journal of Liquid Chromatography* **10,** 1999–2022 (1987).

[20] Schneider, M. & Müllen, K. Hybrid Materials Doped with Covalently Bound Perylene Dyes through the Sol−Gel Process. *Chemistry of Materials* **12,** 352–362 (2000).

[21] Niu, D. *et al.* Preparation of Uniform, Water-Soluble, and Multifunctional Nanocomposites with Tunable Sizes. *Advanced Functional Materials* **20,** 773–780 (2010).

[22] Choi, S.-H., Lee, S.-H., Hwang, Y.-M., Lee, K.-P. & Kang, H.-D. Interaction between the surface of the silver nanoparticles prepared by γ-irradiation and organic molecules containing thiol group. *Radiation Physics and Chemistry* **67,** 517–521 (2003).

[23] Sendroiu, I. E., Warner, M. E. & Corn, R. M. Fabrication of Silica-Coated Gold Nanorods Functionalized with DNA for Enhanced Surface Plasmon Resonance Imaging Biosensing Applications. *Langmuir* **25,** 11282–11284 (2009).

[24] Huang, C. & Hu, B. Silica-coated magnetic nanoparticles modified with γ-mercaptopropyltrimethoxysilane for fast and selective solid phase extraction of trace amounts of Cd, Cu, Hg, and Pb in environmental and biological samples prior to their determination by inductively coupled plasma mass spectrometry. *Spectrochimica Acta Part B: Atomic Spectroscopy* **63,** 437–444 (2008).

[25] Shah, K. W. *et al.* Aqueous route to facile, efficient and functional silica coating of metal nanoparticles at room temperature. *Nanoscale* **6,** 11273–11281 (2014).

7. Appendices

Appendix a.

Lot and Chemical Abstract Service (CAS) on chemicals used

Table. A1 Lot and CAS on chemicals used

Chemical	Lot	CAS
MPTMS	MKBV1975V	4420-74-0
Acetone	1705T031	67-64-1
Polyurethane	SF12303	9009-54-5
Ammonia	K44756432 329	1336-21-6

Appendix b.

TEM images of MNPs and NMOs before (on the left) and after (on the right) coating

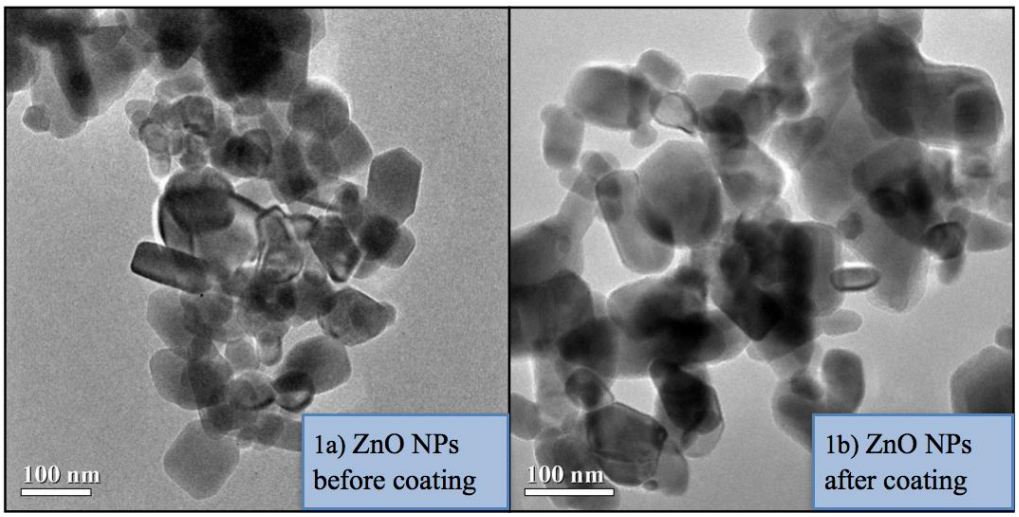

Fig. b1 Unsuccessful coating of ZnO NPs.

TEM image of bare zinc (II) oxide (ZnO) NPs before coating (1a) displays rectangular shapes, with side lengths of ~50-120 nm. TEM image of ZnO NPs after coating (1b) displays less distinct borders, showing possible adherence of MPTMS shell onto the surface of the particles, yet is unmeasurably thin and non-uniform.

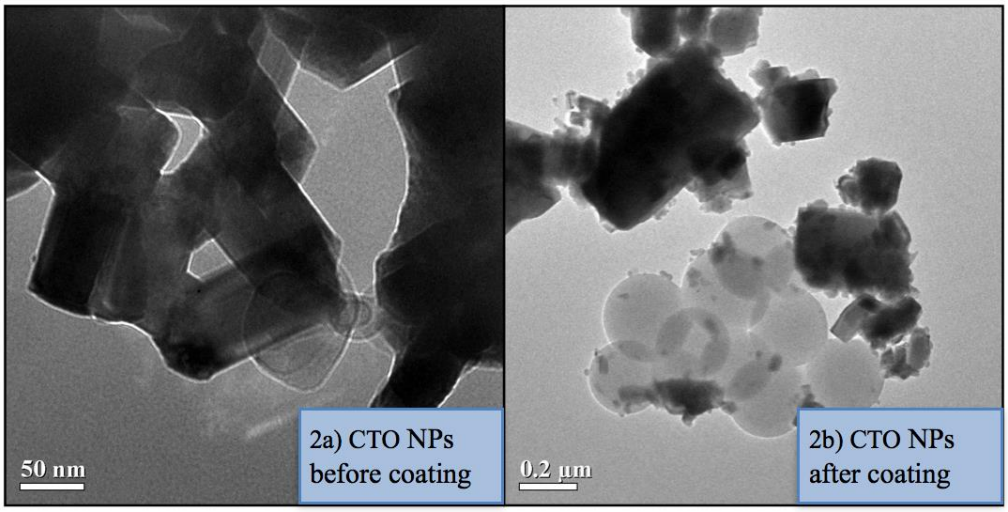

Fig. b2 Unsuccessful coating of CTO NPs.

TEM image of bare cesium tungsten oxide (CTO) NPs before coating (2a) displays rectangular shapes, in dimension of ~60 x 120 nm. TEM image of CTO NPs after coating (2b) displays bare CTO NPs and spherical MPTMS in vicinity to each other yet with minimal or no interaction.

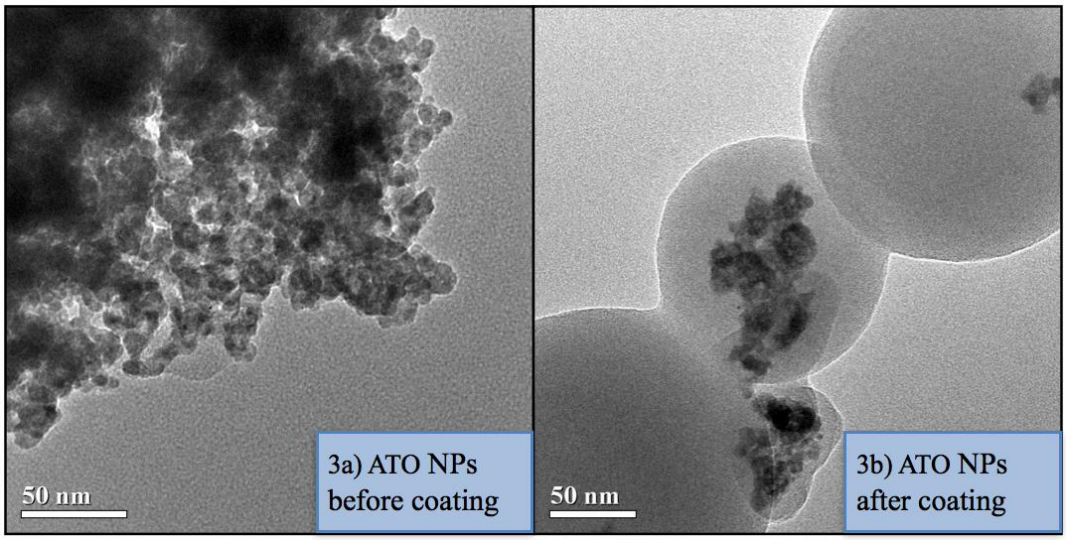

Fig. b3 Successful coating of ATO NPs.

TEM image of bare antimony tin oxide (ATO) NPs before coating (3a) displays granular shape with diameter of ~7.5 nm.

TEM image of ATO NPs after coating (3b) displays ATO NPs being encapsulated in spherical silica shell. The coated ATO NPs are of the diameter between 135nm and 200 nm. However the shell thickness is non-uniform, showing room for improvement in the coating method.

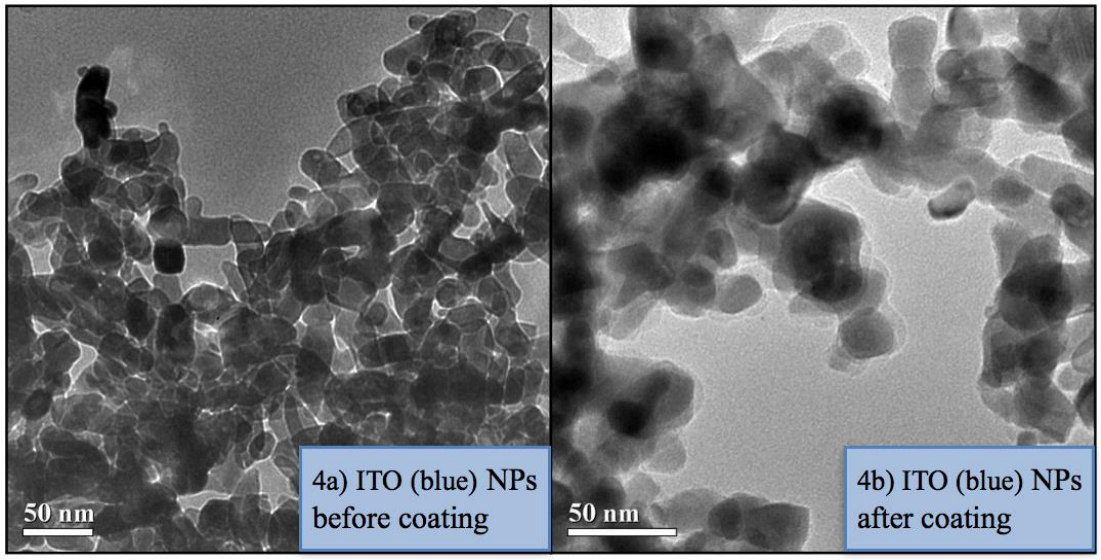

Fig. b4 Unsuccessful coating of ITO (blue) NPs.

TEM image of bare indium tin oxide (ITO) NPs before coating (4a) displays rectangular shapes, with dimension of ~40x15 nm. TEM image of ITO NPs after coating (4b) displays less distinct borders, showing possible adherence of MPTMS shell onto the surface of the particles, yet is non-uniform and barely distinguishable.

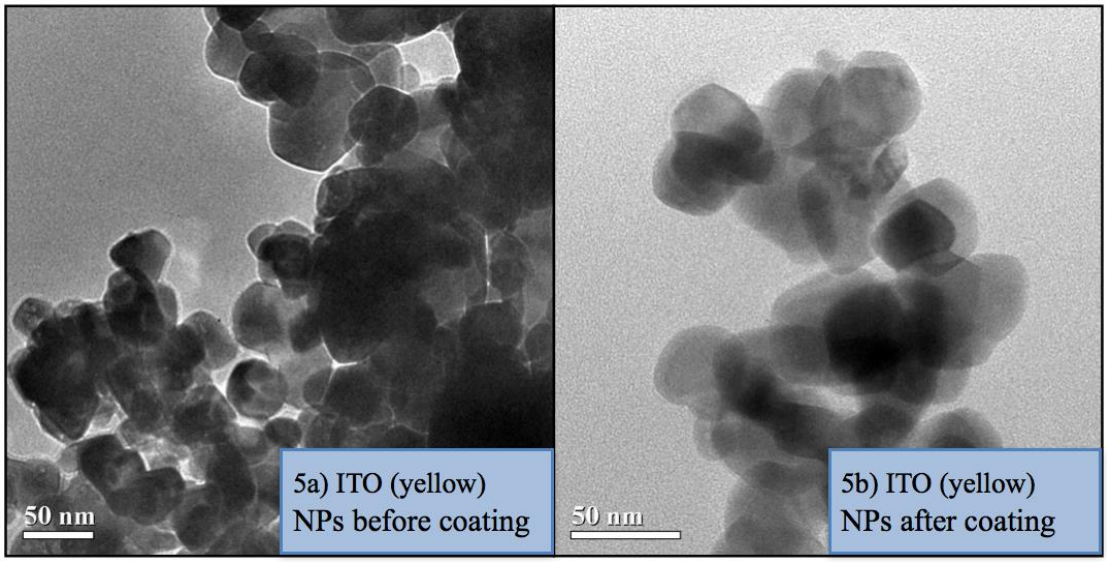

Fig. b5 Unsuccessful coating of ITO (yellow) NPs.

TEM image of bare ITO NPs before coating (5a) displays squarish shapes, with side lengths of ~50 nm. TEM image of ITO NPs after coating (5b) displays less distinct borders, showing possible adherence of MPTMS shell onto the surface of the particles, yet is unmeasurably thin and non-uniform.

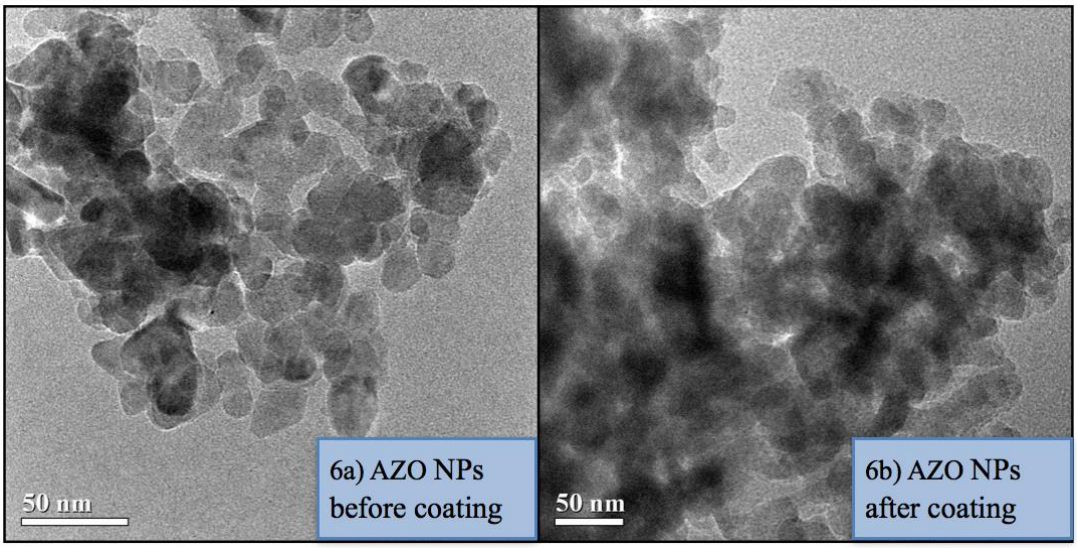

Fig. b6 Unsuccessful coating of AZO NPs.

TEM image of bare aluminium-doped zinc oxide (AZO) NPs before coating (6a) displays irregular polygonal shapes, with side lengths of ~15 nm. TEM image of AZO NPs after coating (6b) displays particles with roughly the same shape and size.

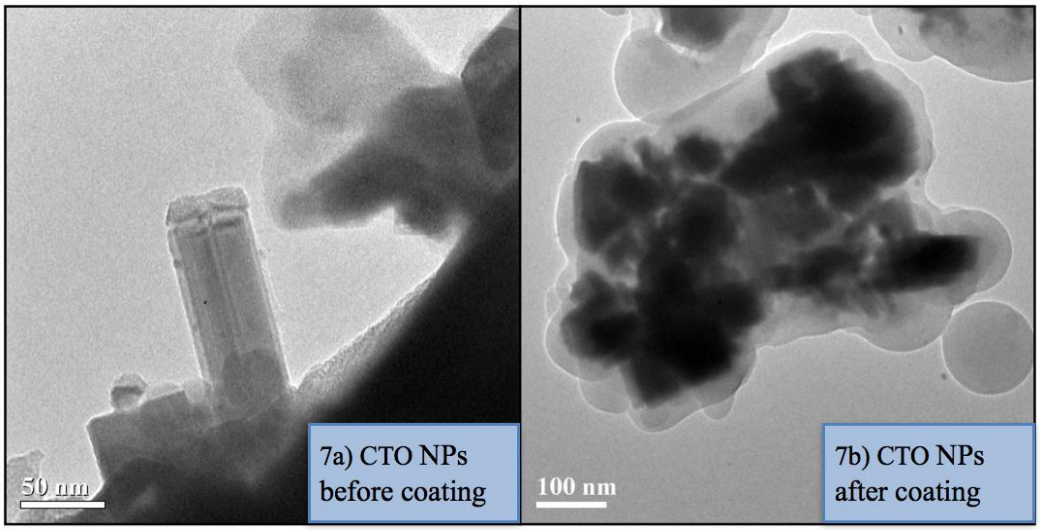

Fig. b7 Successful coating of CTO NPs.

TEM image of bare cesium tungsten oxide CTO NPs before coating (7a) displays rectangular shapes with dimensions of ~150x50 nm. TEM image of CTO NPs after coating (7b) displays CTO NPs being encapsulated in a largely uniform silica shell. The coated CTO NPs displays a rectangular shape with dimension of ~360x530 nm, and shell thickness between 25 and 60 nm.

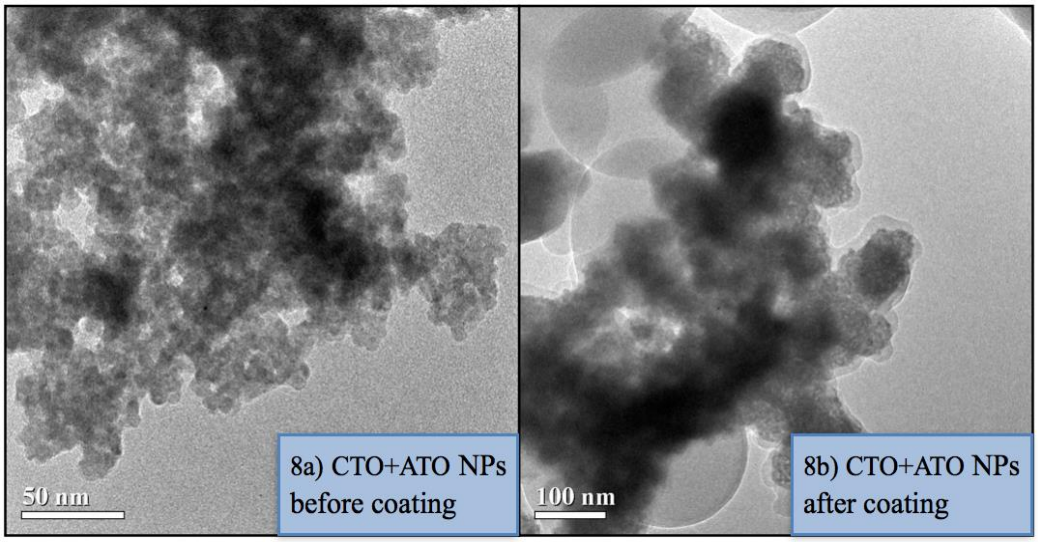

Fig. b8 Successful coating of CTO+ATO NPs.

TEM image of bare CTO+ATO NPs before coating (8a) displays granular shape with diameter of ~7.5 nm. TEM image of CTO+ATO NPs after coating (8b) displays CTO+ATO NPs being encapsulated in silica shell of regular thickness (ignoring the portion being obscured by MPTMS spheres). The coated CTO+ATO NPs shows a shell thickness of 10~200nm. Yet the particles exist in large clusters which may undermine its size-dependent properties, showing room for improvement in the process of preparing NPs.

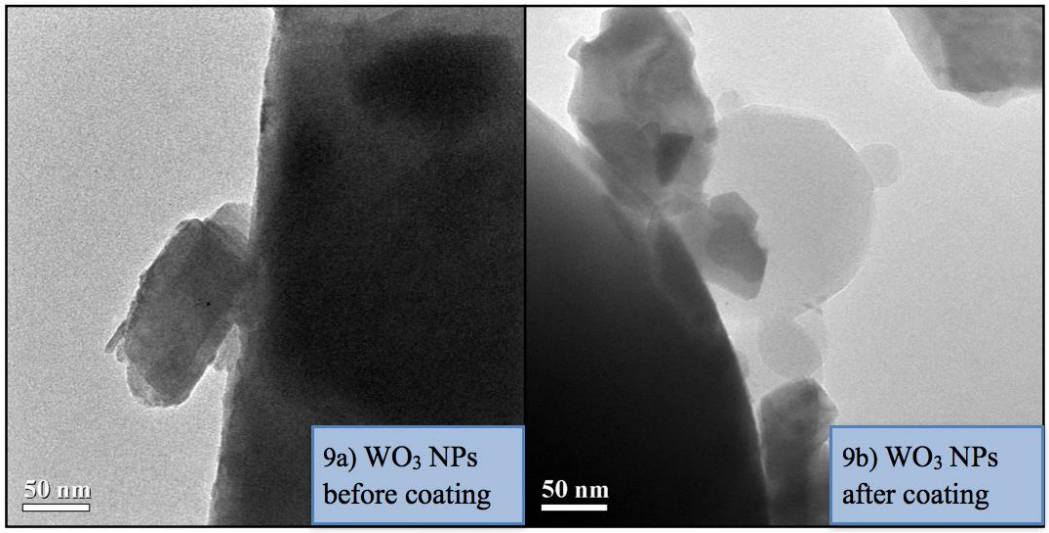

Fig. b9 Unsuccessful coating of WO_3 NPs.

TEM image of bare tungsten trioxide (WO_3) NPs before coating (9a) displays rectangular shapes, with dimensions of ~125x75 nm. TEM image of WO_3 NPs after coating (9b) displays less distinct borders, showing possible adherence of MPTMS shell onto the surface of the particles, yet is unmeasurably thin and non-uniform.

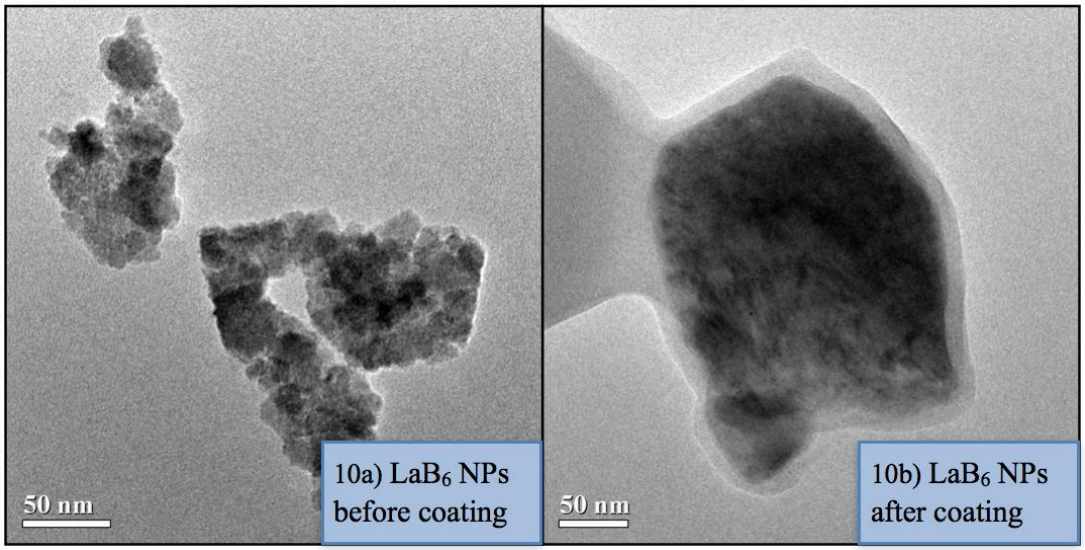

Fig. b10 Successful coating of LaB_6 NPs.

TEM image of bare lanthanum hexaboride (LaB6) NPs before coating (10a) displays spherical shapes with diameter of 10~15 nm. TEM image of LaB_6 NPs after coating (10b) displays LaB_6 NPs being encapsulated in a largely uniform silica shell. The coated LaB_6 NPs displays a rectangular shape with dimension of ~275x230 nm, and shell thickness between 15 nm.

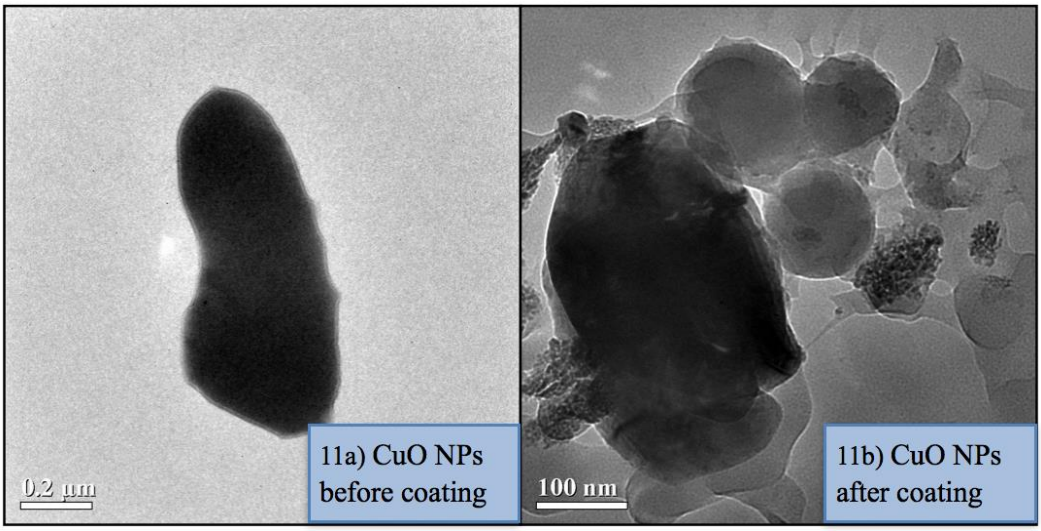

Fig. b11 Unsuccessful coating of CuO NPs.

TEM image of bare copper (II) oxide (CuO) NPs before coating (11a) displays bean shape with length of 1µm, width of 320 nm in the center and 400 nm at the sides. TEM image of CuO NPs after coating (11b) displays a mixture of CuO NPs and MPTMS spheres, showing possible adherence of MPTMS shell onto the surface of the particles, yet is non-uniform.

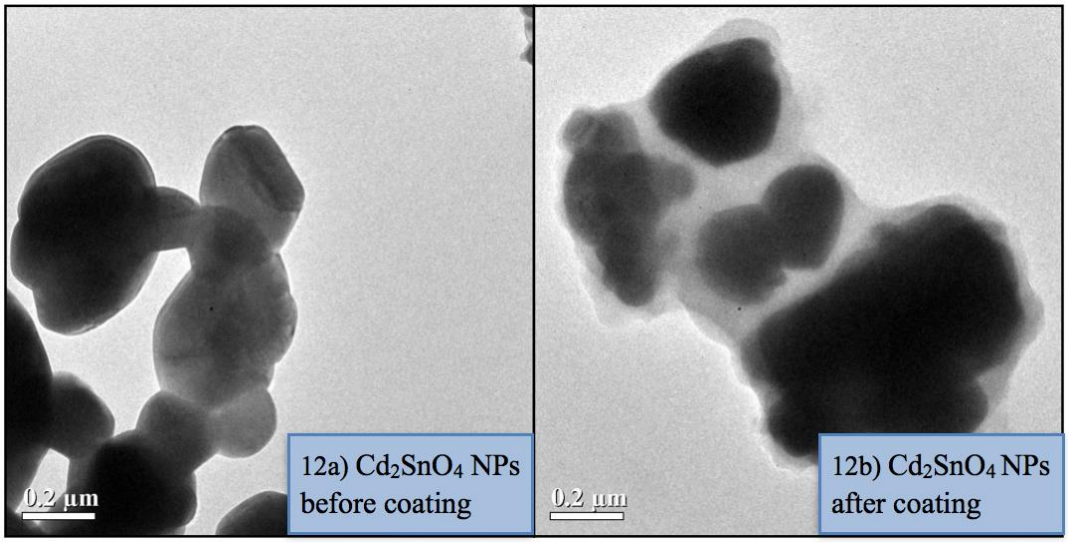

Fig. b12 Successful coating of Cd_2SnO_4 NPs.

TEM image of bare Cd_2SnO_4 NPs before coating (12a) displays irregular spheres with diameter of ~360 nm. TEM image of Cd_2SnO_4 NPs after coating (12b) displays CTO NPs being encapsulated in a largely uniform silica shell. The coated CTO NPs displays a rectangular shape with dimension of ~360x530 nm, and shell thickness between 25 and 60 nm.

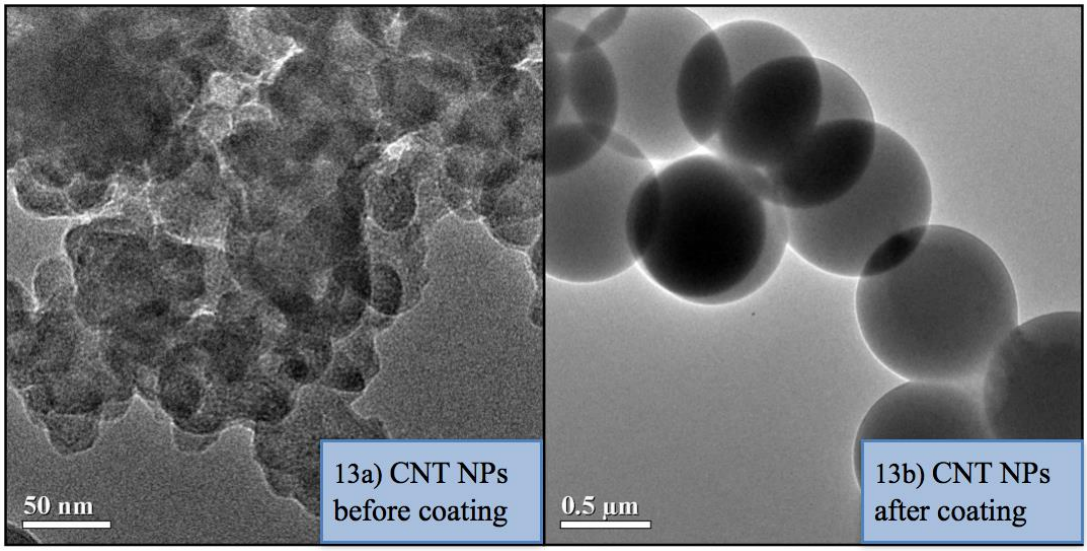

Fig. b13 Unsuccessful coating of CNT NPs.

TEM image of bare carbon nanotube-nanoparticle (CNT) NPs before coating (13a) displays granular shape with diameter of ~30 nm. TEM image of CNT NPs after coating (13b) displays empty MPTMS spheres, suggesting minimal to no interaction between MPTMS and CNT NPs.

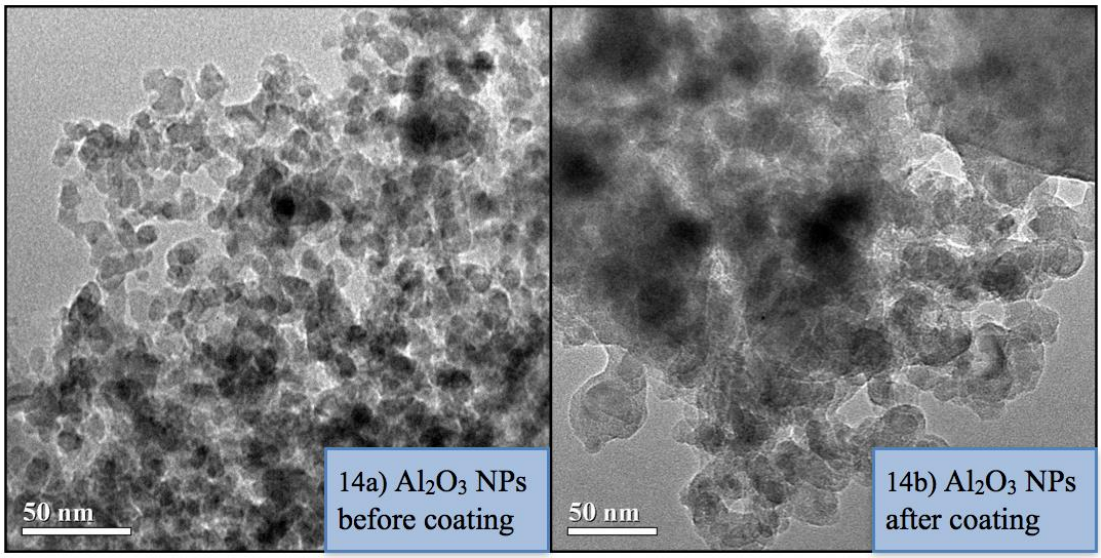

Fig. b14 Unsuccessful coating of Al_2O_3 NPs.

TEM image of bare Al_2O_3 NPs before coating (14a) displays spheres with diameter of 6~10 nm. TEM image of Al_2O_3 NPs after coating (14b) displays spheres with similar size and shape.

Appendix c.

Samples of tested NPs

Fig. c1 Bare NPs in MPTMS; from left to right: Cu , LaB_6, ITO (yellow), ITO (blue), ATO, Cu (vendor Hong Wu), WO_3, CuO, AZO, Al_2O_3, CTO, CTO (NL), $CsWO_3$, CNT, ZnO (Sigma Aldrich) ,ZnO

Fig. c2 NPs reacted with MPTMS in alkaline environment ; sequence same as Fig. c1

Appendix d.

Experiment setups

1. Ultrasonic bath setup

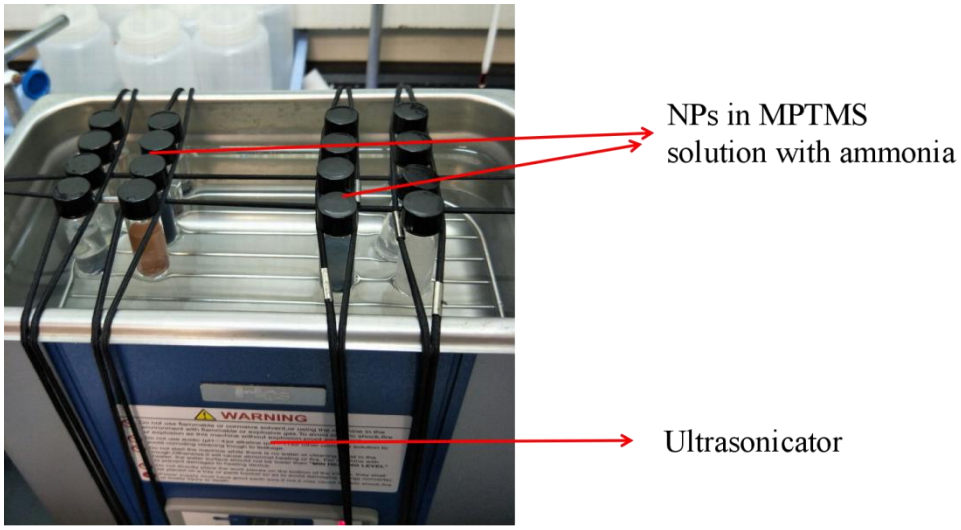

Fig. d1 Ultrasonic bath setup

2. UV-vis-NIR spectroscopy setup

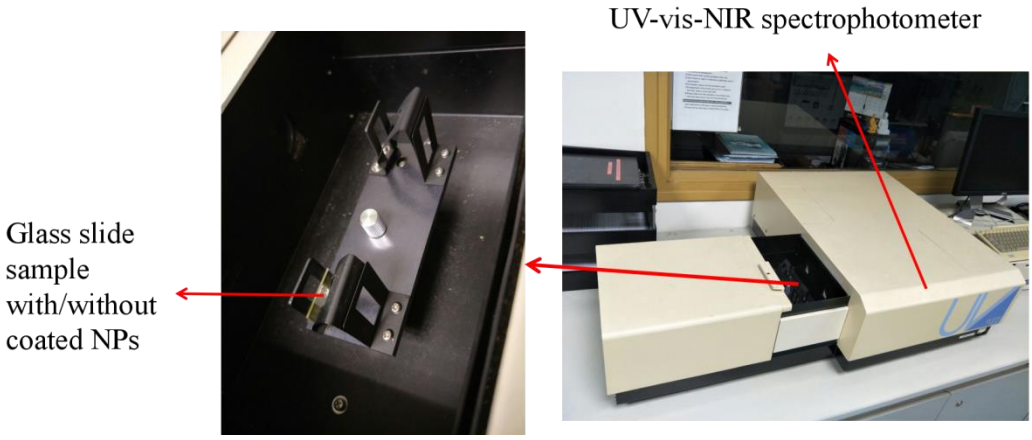

Fig. d2 UV-vis-NIR spectrophotometer setup

3. Infrared imaging setup

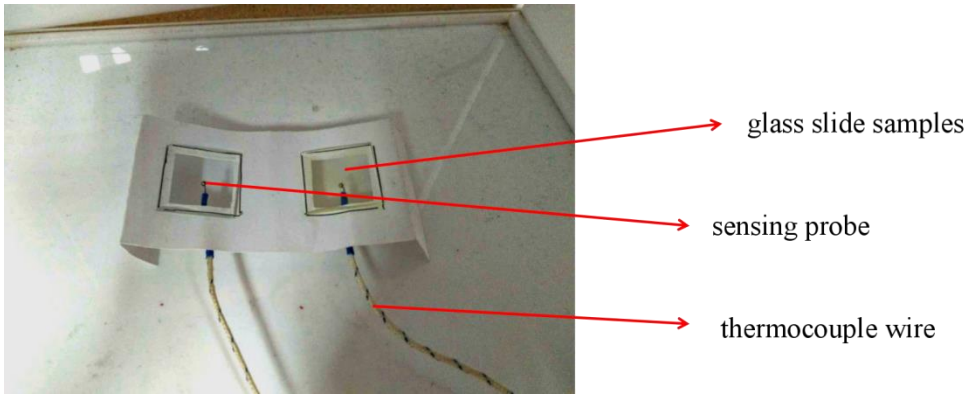

Fig. d3 Thermocouple connector setup

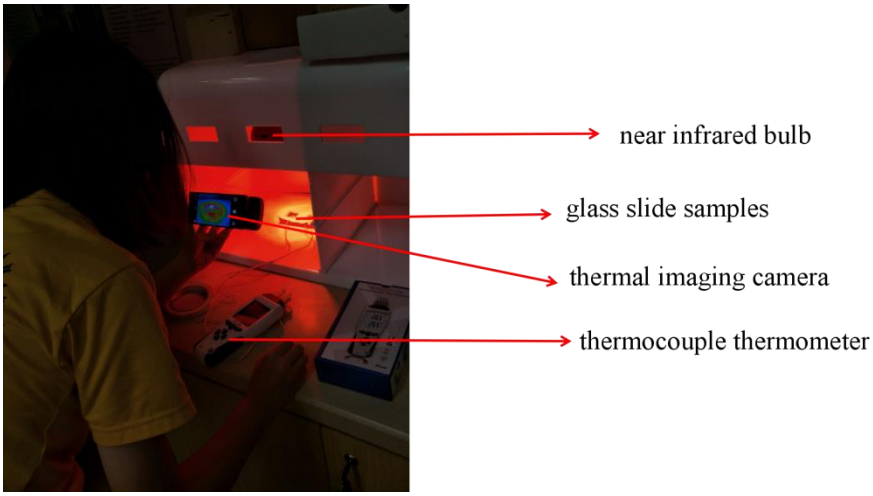

Fig. d4 Infrared imaging setup

4. Temperature change test setup

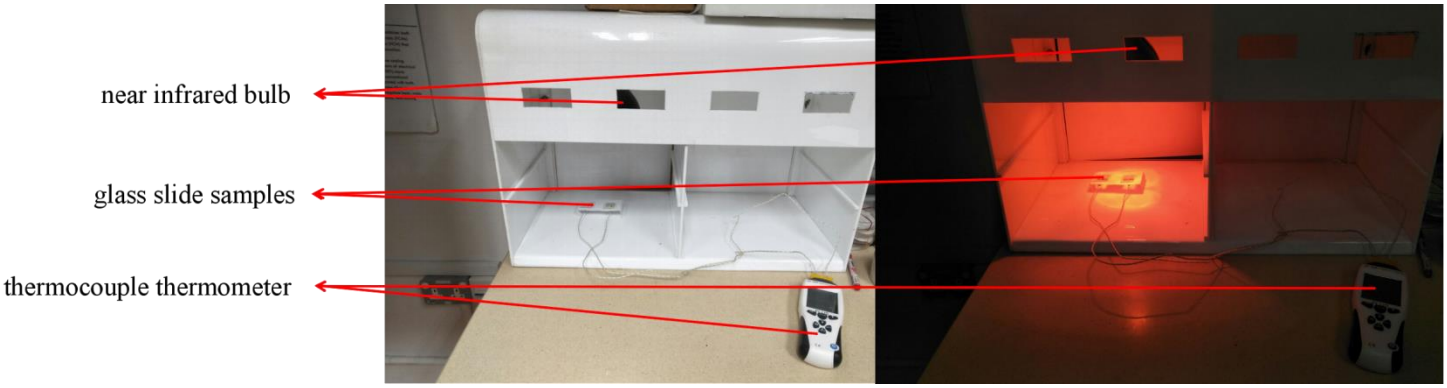

Fig. d5 Temperature change test setup

Appendix e.

Comparison of different reaction accelerating methods

Table. e1 Comparison of Various Shaking Methods Tested

	Advantage	Disadvantage
Ultrasonicator	Relatively Fast	NPs Cluster at the Bottom of the Glass Vial
Shaker	NPs Evenly Distributed	Slow Reaction
Magnetic Stirrer	NPs Evenly Distributed	NPs Stick to the Magnetic Stirrer

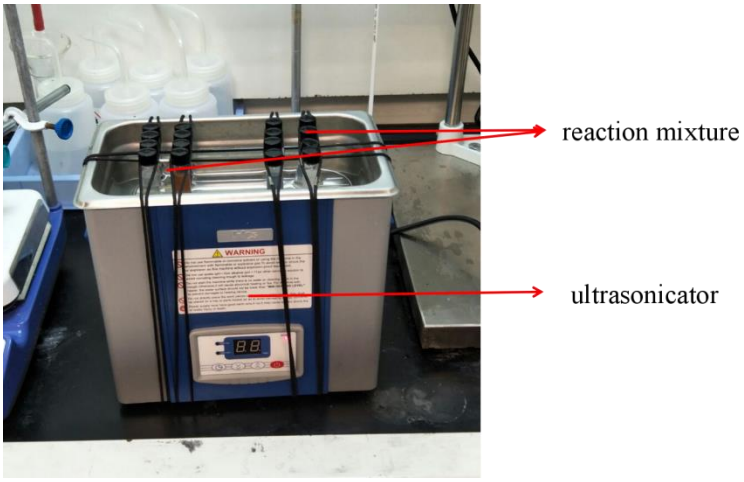

Fig. e2 Experimental setup of ultrasonic bath

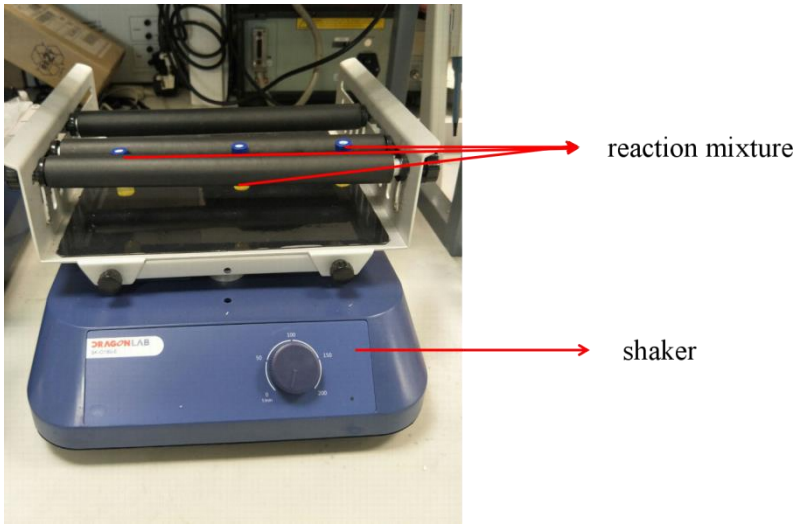

Fig. e3 Shaker

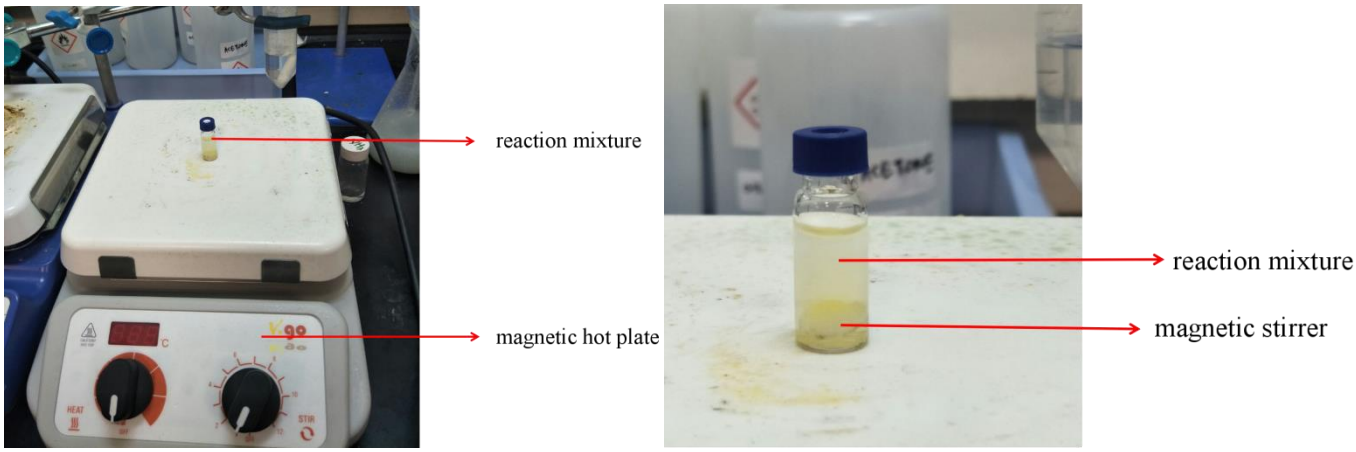

Fig. e4(a)&(b) Magnetic stirrer

Appendix f.

Thermal images of experimental setup exposed to IR heating

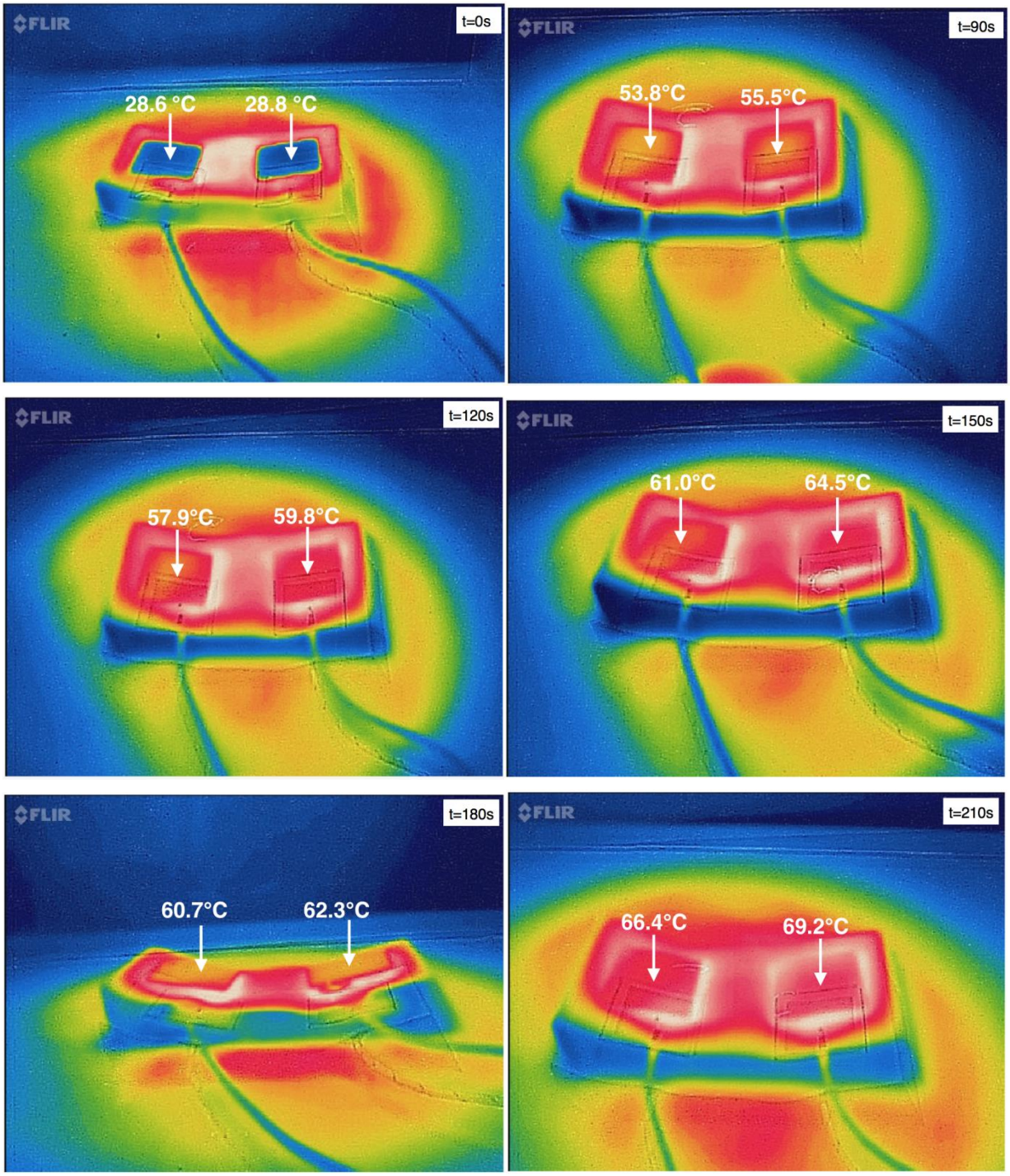

Fig.f1,2,3,4,5,6 Thermal images taken using Flir One when glass slide coated with bare WPU (left) and glass slide coated with Cd_2SnO_4@SiO_2 NPs (right) are placed under IR heating for a duration of 0s, 90s, 120s, 150s, 180s, 210s respectively. The temperatures represented by different colours indicate that glass slide coated with Cd_2SnO_4@SiO_2 NPs consistently absorbs more heat than the glass slide coated with bare WPU. Thus Cd_2SnO_4@SiO_2 NPs can be concluded to have novel heat absorbing effect when applied onto building materials. Fig.f5 is

identified as an anomaly as the temperatures of both glasses showed a decrease from 30s ago, possibly because of the angle from which the thermal image was taking.

Appendix g.

Tables showing temperature difference during temperature change test

Table. g1 Temperature change of glass during heating

Time/s	Temperature of Glass without NPs/°C	Temperature of Glass with Coated NPs/°C	Temperature Difference/°C
0	29.3	29.3	0
20	36.3	36.8	0.5
40	40.6	41.6	1.0
60	44.2	45.5	1.3
80	48.2	49.9	1.7
100	51.5	53.1	1.6
120	54.2	56.9	2.7
140	55.3	57.7	2.4
160	57	59.5	2.5
180	58.8	60.2	1.4

Table. g2 Temperature change of glass during heating

Time/s	Temperature of Glass with Uncoated NPs/ °C	Temperature of Glass with Coated NPs/°C	Temperature Difference/°C
0	24.8	24.8	0
20	32.4	34.6	2.2
40	37	40.6	3.6
60	40.8	45.7	4.9
80	43.6	49.4	5.8
100	46.3	53.3	7
120	48.9	56	7.1
140	50.9	58.6	7.7
160	52.7	60.4	7.7

Table. g2 Temperature change of glass during heating

Time/s	Temperature of Glass without NPs/°C	Temperature of Glass with Coated NPs/°C	Temperature Difference/°C
0	27.3	27.3	0
20	39.6	37.4	2.2
40	46.2	43.3	2.9
60	50.4	46.8	3.6
80	53.3	49.2	4.1
100	55.3	52.5	2.8
120	54.2	50.4	3.8
140	53.2	48.8	4.4
160	55.1	50.9	4.2
180	59.5	54.7	4.8
200	59.7	56	3.7

Table. g4 Temperature change of surrounding air

Time/s	Temperature of Glass with Uncoated NPs/ °C	Temperature of Glass with Coated NPs/°C	Temperature Difference/°C
0	30.7	30.6	0.1
20	37.9	36.7	1.2
40	44.3	42.4	1.9
60	49.4	47.3	2.1
80	52.1	50.1	2.0
100	55.2	52.9	2.3
120	56.1	54.8	1.3
140	57.9	56.2	1.7